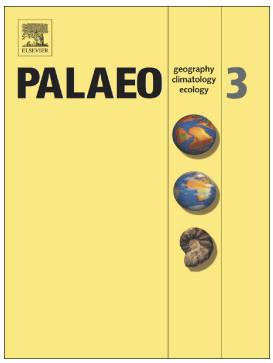

The evolution of microbialite forms during the Early Triassic transgression: A case study in Chongyang of Hubei Province, South China

Tan Wang, Robert V. Burne, Aihua Yuan, Yongbiao Wang, Zhixing Yi

PII: S0031-0182(17)31086-6
DOI: https://doi.org/10.1016/j.palaeo.2018.01.043
Reference: PALAEO 8652

To appear in: *Palaeogeography, Palaeoclimatology, Palaeoecology*

Received date: 26 October 2017
Revised date: 30 January 2018
Accepted date: 31 January 2018

Please cite this article as: Tan Wang, Robert V. Burne, Aihua Yuan, Yongbiao Wang, Zhixing Yi , The evolution of microbialite forms during the Early Triassic transgression: A case study in Chongyang of Hubei Province, South China. The address for the corresponding author was captured as affiliation for all authors. Please check if appropriate. Palaeo(2017), https://doi.org/10.1016/j.palaeo.2018.01.043

The evolution of microbialite forms during the Early Triassic transgression: a case study in Chongyang of Hubei Province, South China

Tan Wang[a], Robert V. Burne[b,c], Aihua Yuan[a], Yongbiao Wang[a]*, Zhixing Yi[a]

[a] *State Key Laboratory of Geological Processes and Mineral Resources, School of Earth Sciences, China University of Geosciences, Wuhan 430074, China*

[b] *The Australian National University, Research School of Earth Sciences, Australia*

[c] *University of Queensland, School of Earth and Environmental Science, Australia*

**Corresponding author: Tel.: + 86 27 6788 4320; fax: +86 27 6788 3001; E-mail address: wangyb@cug.edu.cn (Y. Wang).*

Abstract The widespread development of microbialites in shallow areas of the Tethys Ocean at the start of the Early Triassic reflects the deterioration of marine ecosystems in the aftermath of the extinction that marked the demise of the majority of Palaeozoic marine faunas. Here we present a study of the evolving microbialite forms and associated biotic assemblages of this pioneering microbialite interval from exposures at Chongyang, Hubei Province, China. This research provides a perspective on the effects of eustatic transgression on marine ecosystems as water depths increased at the beginning of Mesozoic, through the study of the changing forms, microfacies and distribution of microbialites. Microbialite forms evolved from stratiform stromatolites to a sequence of tabular thrombolites (with an intercalated layer of columnar stromatolites), followed by domical thrombolites that were overlain, in turn, by oolites. The stratiform stromatolites contain poorly preserved remains of calcified cyanobacteria, but microfossils with chambered structure can also be seen. Metazoan fossils increased from the base of the overlying tabular thrombolite, reflecting increasing biodiversity with deepening of seawater. The occurrence of columnar stromatolites within the tabular thrombolite may indicate a temporary sea-level shallowing. Foraminiferans and other metazoans are absent within the columnar stromatolites, but spherical cyanobacterial remains are extremely abundant. Well-preserved calcified cyanobacteria may reflect an absence of metazoan predation and/or carbonate supersaturation of seawater. As water deepened, domical thrombolites developed and the more complex seafloor relief created varied niches between and within the domes that harboured more ecologically diverse

communities. During the process of transgression within the microbialite interval, carbon isotopes exhibit a negative relationship with biodiversity, implying that upwelling of anoxic deep-ocean water, if associated with the negative excursion of carbon isotope values, did not inhibit the diversification of benthic organisms at least on shallow carbonate platforms in the period immediately after the end-Permian mass extinction.

Keywords: Stromatolite; Thrombolite; Mass extinction; Transgression; Palaeoecology; Carbon isotope

1. Introduction

The end-Permian global event devastated both terrestrial and marine ecosystems (Algeo et al., 2011, and references therein). In shallow marine environments, a great regression at the end of the Permian resulted in the exposure and extensive erosion of carbonate platforms (Newell, 1967; Heydari et al., 2003; Wu et al., 2003; Wu et al., 2010; Farabegoli and Perri, 2012; Yin et al., 2014), which magnified the effects of biotic mass extinction. In South China, these platforms were re-submerged at the start of Early Triassic that is marked by the first occurrence of conodont fossil of *Hindeodus parvus* (Yin et al. 2001; Jiang et al., 2014; Wang et al., 2016). During this Early Triassic transgression microbialites developed over large areas of the Yangtze Platform as well as elsewhere around the world (Kershaw et al, 1999; Lehrmann, 1999; Lehrmann et al., 2003; Ezaki et al., 2003; Wang et al., 2005; Baud et al., 2007; Liu et al, 2007; Kershaw et al, 2012; Wu et al., 2014; Wu et al. 2016; Fang et al., 2017; Wu et al., 2017). Microbialites dominated the depleted shallow-marine ecosystems in the aftermath of end-Permian mass extinction (Wang et al., 2005; Wu et al., 2007). Research on their sedimentology and geochemistry (Lehrmann et al., 2003; Luo et al., 2010; Liao et al., 2017) has generally regarded the microbialites as a single unit. The details of this dramatic ecological change and development remain unclear despite studies clearly demonstrating that microbialite form varies from place to place, and both internal fabric and associated microfossils change from the bottom to the top of this interval (Ezaki et

al., 2003; Liu et al., 2007; Kershaw et al, 2012). A closer inspection shows the microbialite interval is composed of several different microfacies that preserve important evidence of the evolution of the marine ecosystem. Here we report a case-study of the development of this microbialite interval preserved in the Chongyang section of Hubei Province (about 10 km to the east of Chongyang County, 29°31'56"N, 114°10'37"E). This section shows how microbialite form developed as the transgression progressed. Due to the close relationship between the microbialite form, ecosystem diversity and water depth, this sequence of microbialites provides valuable clues to the evolution of shallow-water ecosystems in the aftermath of the end-Permian mass extinction. Carbon isotope analyses were also undertaken along the section to probe the possible relationship between marine chemistry, sea-level change and microbialites development during the transgression.

2. Geological background

Two contrasting sedimentary facies associations co-exist in the Late Permian Changhsingian of the South China Block (Fig. 1): shallow-water carbonate platform deposits and muddy, siliceous, deep basinal deposits. The end-Permian regression resulted in the exposure and erosion of shallow platforms that were then re-colonized by microbial carbonates during the subsequent Triassic transgression. These microbialites evolved through morphologically comparable sequences in sections exposed at several geographical locations on the platforms (Kershaw et al., 2012). We describe here a typical section, the Chongyang section in Hubei Province. We analyze the relationship between the variation of microbialite forms with increasing ecosystem diversity, and with carbon isotope variations during the Early Triassic transgression.

The Chongyang section lies on the northern margin of Yangtze carbonate platform (Fig. 1). The stratigraphic sequence of Permo-Triassic interval in Chongyang section is very clear. This region was a typical shallow-water platform environment during the Late Permian Changhsingian and was characterized by the deposition of grainstones enriched in calcareous algae and foraminiferans. The top of these Permian grainstones is now an undulating surface. This is capped by residual deposits enriched in ferric oxide that probably represents the weathering and erosion products that formed on the

platform following its exposure by the regression. The erosion surface is now overlain by a 10-m-thick interval of microbialites that formed during the transgression at the beginning of base of the Triassic (Fig. 2), which then passes upward into a sequence of oolites.

The Changxing Formation of Late Permian is composed of a bioclastic grainstone containing a rich and diverse fossil assemblage of benthic organisms. The time of deposition of the top Permian grainstone clearly precedes the final stage of the Permian while the bottom of the microbialite interval marks the onset of the Mesozoic transgression. The overlying Early Triassic facies sequence indicates dramatic change in the marine ecosystem, and is dominated by microbialites. The conodont species *Hindeodus parvus* was originally reported within the microbialite interval, but recent detailed work indicates that this conodont fossil is actually present in sediments at the bottom of the microbialite interval in many sections across South China (Liu et al., 2007; Jiang et al., 2014; Wang et al., 2016). Therefore, the Permo-Triassic boundary in this section is assigned to the bottom of microbialite interval.

This microbialite interval can be subdivided into four members comprising, from bottom to top: 1) a 20-cm-thick unit of stratiform stromatolites; 2) tabular thrombolites interbedded with thin-bedded bioclastic limestone and a single 10-cm-thick unit of columnar stromatolites; 3) domical thrombolites with abundant interspace fillings rich in fossil fragments; 4) oolitic limestone.

3. Methods

Hydrochloric acid was used to wash the surface of different forms of microbialites to provide a large, clear area of outcrop for study. Large samples of typical microbialite forms were taken with a portable power saw machine to enable a detailed study of macro-structure in the microbialites. Micro-fabrics of the samples were examined under an optical microscope. Due to the minute size of microbial fossils, a scanning electron microscope was used to reveal and photograph their structure.

The aftermath of end-Permian mass extinction is generally marked by a global negative excursion of carbon isotopes. For the purpose of comparison with other sections, high-resolution fresh samples were collected from both the topmost Permian

limestone and the Triassic microbialite interval. Fresh rock chips were chosen and crushed to less than 100 mesh. The carbonate carbon isotope compositions were determined according to McCrea (1950). The sample powder was reacted offline with 100% H_3PO_4 for 24 h at 25° C under vacuum conditions. The isotope composition of the generated CO_2 was measured on a Finnigan MAT 251 mass spectrometer in the State Key Laboratory of Geological Processes and Mineral Resources of China University of Geosciences (Wuhan). All isotopic data are reported as per mille (‰) relative to Vienna Pee Dee belemnite (V-PDB) standard. The analytical precision is better than ±0.1‰ for $\delta^{13}C$.

4. Results

4. 1 Facies sequence and morphological variation of microbialites

The ~10 metre thick Early Triassic microbialite facies sequence in the Chongyang section consists of a succession of microbialite forms, with stratiform stromatolites at the base, followed by tabular thrombolites and then domical thrombolites. This sequence passes sharply upward into an oolitic limestone (Fig. 3). Thin section examination indicates that microfaunal assemblages alter with changing in microbialite form, indicating a relationship between evolving microbialite texture and form with the development of increasing complexity in benthic ecosystem. These changes have the potential to shed light on the impacts of an increasingly diverse shallow-marine ecosystem as well as hydrodynamic conditions as the transgression proceeded from the very beginning of Early Triassic. They are unlikely to be solely due to the effects of increasing predation (such as that suggested by Walter and Heys, 1985).

4.1.1 Stratiform stromatolite facies

A 20-cm-thick stratiform stromatolite formed above the erosion boundary in Chongyang section at the beginning of the Early Triassic transgression (Fig. 4A). This stromatolite facies is laterally extensive with the laminated structures being clearly discernable in widespread outcrops. Poorly preserved mineralized remains of the original microbial community can be readily found within the stromatolite fabric, with possible cyanobacteria fossils clearly exhibiting chambered structures (Fig. 4B and C).

There are no hydrodynamic sedimentary structures, indicating that the persistent parallel laminations reflect accretion from benthic microbial mats rather than deposition from turbulent water currents. Metazoan fossils are rare in the stromatolite stage. Infrequent ostracods and gastropods were probably transported in from elsewhere. Thin-shelled foraminiferan *Globivalvulina* is commonly found. This species is known from the Permian and was able to survive the end-Permian mass extinction (Luo et al., 2013). It is one of the so-called "*disaster species*" that exhibit strong adaptive capabilities that enabled them to survive the extinction.

Stromatolites can exhibit a variety of forms that may reflect hydrodynamic conditions. Many researchers reported columnar stromatolites occur in the lower intertidal or subtidal zones, while the stratiform stromatolites tend to form in the upper intertidal or even supratidal environment (Glumac and Walker, 1997; Jahnert and Collins, 2013; Burne and Johnson, 2014). However, desiccation features, mudcracks, roll-up structures and other features typical of supratidal microbial mat deposits are not present, so it is reasonable to infer that this facies was deposited in a very shallow, tranquil, and possibly intertidal environments at the very beginning of Early Triassic transgression.

4.1.2 Tabular thrombolite facies

This facies is dominated by tabular thrombolites but also contains a single 10-cm-thick lenticular layer of columnar stromatolite. Thin section analysis indicates that the thrombolites are composed of micritic parts and coarser-crystalline parts which were interpreted as the possible cast fossils similar to those described by Wu et al. (2014) as the colonies of the cyanobacterium *Microcystis*. In contrast with the underlying stratiform stromatolite facies, many metazoan fossils are found within the thrombolites. These include abundant ostracods, worm tubes and small gastropods (Fig. 5). These fossils vary in abundance but show low diversity and are considered to be reworked material that accumulated as interbeds between the tabular thrombolites.

Stromatolites first appeared in the early Archean (Nutman et al., 2016), while the thrombolites occur for the first time in the Mesoproterozoic (Zhang et al., 2016). The rise of thrombolites was originally thought to be a consequence of increasing metazoan

predation (Walter and Heys, 1985) based largely on the observed disruption of inter-tidal microbial mats by gastropods in the Bahamas (Garrett 1970). However studies of modern thrombolites from Hamelin Pool (Monty, 1976) and Lake Clifton (Moore and Burne, 1994) have revealed that thrombolites form, not simply a result of predation, but rather through balanced competitive interaction between microbial communities, algae, plants and animals within complex ecosystems comparable to those of coral reefs. Thrombolites would necessarily require a suitable water depth to form to sustain this ecological diversity, especially considering the extremely high temperatures inferred in the aftermath of the end-Permian mass extinction (Sun et al., 2012).

A 10-cm-thick lenticular layer of columnar stromatolites is interbedded within the tabular thrombolites at this facies (Fig. 6A). Forams and other metazoan fossils are scarce within the columnar stromatolites, but they contain well-preserved, hollow, spherical microbial fossils (Fig. 6B, C) interpreted as the remains of coccoidal microbes (Ezaki et al., 2003; Yang et al., 2011; Adachi et al., 2017). The diameter of single coccoid is about 20-30 μm, and assemblages of several coccoid microfossils appear in clusters and are arranged along the laminae. Similar spherical microfossils were also reported in Laolongdong section of Chongqing, where they were compared with the extant epiphytic cyanobacterium *Stanieria* (Wu et al., 2016).

The occurrence of a bed of stromatolites within this thrombolitic facies suggests a short-term shallowing of the environment that limited biological diversity (Glumac and Walker, 1997). One possible explanation for this might be that, under high temperature conditions（Sun et al., 2012）, strong evaporation would more likely affect shallow water environments, leading to hypersalinity that favoured the growth of stromatolites, but inhibited other organisms (Zhu et al., 1993). Hypersalinity not only limits ecological diversity but also creates favorable chemical conditions that facilitate the calcification of cyanobacteria, and calcified cyanobacteria have been found within the stromatolites deposited in hypersaline conditions (Pratt, 1984).

4.1.3 Domical thrombolite facies

Thrombolites of this facies are organized as domical mounds (Fig. 7A). The smaller domes are about 30-40 cm in size, while the large ones can reach more than 1 m. The

morphological characteristic can be seen clearly in plane view at an equivalent horizon in a nearby section which has ever been studied by Adachi et al.(2017) although the domes are much smaller there (Fig. 7B). The irregular interspace between domes was filled with sediments (Fig. 7A) rich in brachiopods, gastropods and other fossil fragments (Fig. 7C). This contrasts with the stratiform bioclastic sediments intercalated with the tabular thrombolites in the underlying facies.

Although modern thrombolites have been recorded from both the intertidal zone and the shallowest subtidal zone (Moore and Burne 1994; Jahnert and Collins, 2013), the domical forms require a submerged environment (Moore and Burne 1994; Gleeson et al., 2016). In Bahamas, large columnar thrombolites are found even down to a depth of 8 m (Planavsky and Ginsburg, 2009). We suggest that the occurrence of domical thrombolites associated with a more diverse fossil assemblage in the Chongyang section reflects further deepening of water. In addition to the contrast in morphology, thrombolites in this stage show significant differences in their structure when compared with the underlying tabular thrombolites. Both the size and the proportion of coarser-crystalline parts are greater in the domical thrombolites and the proportion of micritic patches is smaller (Fig. 3). This transformation of thrombolite structure probably reflects the hydrodynamic change from low energy to higher energy. Based on the study of Cambrian thrombolites in California and Nevada in America, Theisen and Sumner (2016) suggested that different mesoscale organizations of micritic clusters probably reflect local variations in the depositional conditions from quiet water to high-energy flows.

It is interesting that the biodiversity and proportion of bigger fossils increases significantly in the interstitial sediments between domes. We suggest that this reflects increasing ecological diversity in deeper water. The complex submarine relief of interspace between domes creates a variety of ecological niches that provides more diverse habitats available for benthic organisms. A similar scenario can be found in modern Lake Clifton of Western Australia, where the complex environments between thrombolites serve as small “reef” ecosystems that harbor a diverse and abundant metazoan fauna (Moore and Burne, 1994).

4.1.4 Oolitic limestone facies

Following the disappearance of thrombolites, an oolitic limestone was deposited (Fig. 8). These limestones consist of poorly sorted ooids set in a micrite matrix. Some of the ooids have irregular, concentric laminae resembling those of oncoids.

The disappearance of microbialites and the rapid transition to an oolitic facies indicates a significant change in the marine environment. Most modern marine ooids are found in warm waters and wave or current agitated settings (Diaz et al., 2015). However Diaz et al. (2015) and O'Reilly et al. (2017) have shown that different ooid types reflect different environmental settings with polished, well-sorted ooids in high energy areas and poorly-sorted, biofilm encrusted ooids in more tranquil environments. Well-sorted pure ooids in the modern Persian Gulf were reported in the water depth of 2 m (Loreau and Purser, 1973), while the ooids in the Great Bahama Bank (GBB) can reach to the depths of 8 m and deeper (Dill et al. 1986). Blackened relict ooids are still common in the 100 m-deep center of the basin in the Persian Gulf (Loreau and Purser, 1973). The ooids overlying the microbialites in Chongyang section are poorly sorted and the interspace among them was filled with much micrite matrix, reflecting either a deeper and/or a more tranquil environment. Although ooids are commonly thought to have been formed in agitated environments, both analysis of pene-contemporaneous oolite sequences in Early Triassic sections at Haicheng and Moyang (Li et al., 2017) and recent theoretical evidence indicate that ooids do not necessarily require agitation for their formation (Batchelor et al., in press). In addition, some ooids possess the irregular concentric laminae comparable to oncolites, again indicating the relatively quiet water environment, consistent with the evidence from other sections in South China (Deng et al., 2017). Thus, the transition from thrombolites to oolites can be interpreted as the result of further deepening of the environment during the post-extinction transgression (Kershaw et al., 2012).

4.2 Isotopic data

A total of 54 samples from different carbonate rocks in Chongyang section were used for carbon isotope analysis with the data presented in Table 1. The results show that the maximum recorded negative value of $\delta^{13}C$ does not occur at the bottom of the

microbialite interval but at a horizon 2.6 m above this (Fig. 3), reflecting a gradual negative excursion of $\delta^{13}C$ with increasing water depth during the Early Triassic transgression. This contrasts with some deep-water sections where a significant negative excursion of carbon isotope commonly occurs just above the end-Permian extinction boundary that is followed by an increasingly positive excursion (Xie et al., 2017).

The differentiation in the carbon isotope records between shallow-water platform and deep-water basin may be related to the hydrochemical heterogeneity of seawater, or the loss of strata near the extinction boundary due to the erosion. The major end-Permian regression resulted in variable degrees of erosion of shallow-water platform in different localities. Therefore, the complete record of carbon isotope variation in the earliest period after the extinction is not recorded in the deposits of the shallow-water platforms but rather in deep-water sections that preserve a complete sedimentary sequence. Isotopic correlation between sections deposited in different water depth should be analysed with caution. Although comparison between microbialite-bearing sections points to a similar negative pattern within the microbialite interval, slight difference can still be seen (Luo et al., 2011). This implies the carbon isotope value might have been modified by local influences although the excursions are supposed to indicate ocean-wide changes.

5. Discussion

5.1. Depositional model for the evolution of microbialite sequence

The sequence described above records the evolution of microbialite forms and associated fossil assemblages during the Early Triassic transgression. At the base of the sequence, there are abundant microfossils (most likely cyanobacteria) along with the protozoan *Globivalvulina*, but the scarcity of metazoans within the stratiform stromatolites implies stressed conditions, perhaps in extremely shallow environments. However, the occurrence of metazoan fossils such as ostracods and gastropods from the start of the tabular thrombolite indicates that environmental conditions had become suitable for the survival of metazoans. This may have been a consequence of the protection of increased water depth from extremely hot climate conditions. This is supported by the biodiversity of metazoans (especially brachiopods) significantly

increasing along with the deposition of domical thrombolite. It is noteworthy that, ecologically, brachiopods generally inhabit relatively deeper water environments than the gastropods (Enay, 1993).

A similar relationship between microbialite form and water depth has been recorded in other geological stages (Glumac and Walker, 1997) as well as in modern marine environments (Feldmann and Mckenzie, 1998; Burne and Johnson, 2012; Suosaari et al., 2016). Thus, based on the analysis of microfacies and the comparison with microbialites in other geological periods as well as in the modern environments, we propose a depositional model for the relationship between microbialite forms and sea-level change during the global transgression in Early Triassic (Fig. 9).

This model clearly implies that sections located in different palaeogeographical settings will have different sequences due to the different arrival time of transgression. We have compared these trends in several sections from various localities on the Triassic platforms of South China (Fig. 10). For example, in Laolongdong section of Chongqing, and in Jianshuigou section (Fig. 10) as well as in the nearby Dongwan section (Ezaki et al., 2003; Kershaw et al., 2007) of Sichuan Province, two different thrombolites can be observed with the tabular thrombolite underlying the domical one. Similarly, the microbialite sequence in Xiushui section of Jiangxi Province (Fig. 10) is composed of tabular thrombolites and overlying dendrolite with no stromatolite at the base (Wu et al., 2017). However, our observations suggest that these overlying dendrolites appear sometimes in the form of domical microbialites with digitate structures. It is interesting to note that in all these sections microbialites are located above a Permian limestone that contains reef facies (Wang et al., 1994; Fan et al., 1996; Xu et al., 1997). Relatively higher relief of reef facies may be the main explanation for the late arrival of Early Triassic transgressive deposits and therefore the absence of stromatolites. By contrast, the Xiajiacao section in the western Hubei Province (Fig. 10) and the Zuodeng section of Guangxi Province (Fig. 10) exhibit a different kind of sequence with a stromatolite bed at the base and thrombolites in the middle and upper parts (Fang et al., 2017; Pei et al., 2017). The Chongyang section described in this paper, however, was deposited in a little deeper environment adjacent to the northern basin

(Fig. 1). Consequently, the microbialite interval preserves a relatively complete sequence with stromatolites, tabular thrombolites and domical thrombolites (Fig. 10). In western Tethys, a similar but more complex sequence developed in the Çürük Dag section of southern Turkey, where a layer of stromatolites formed near the base of the microbialite interval while thrombolites are in the upper part (Kershaw et al., 2011). In the sections from the eastern Tethys, oolite is always deposited after the thrombolite, but in the western Tethys, a thin bed of oolite occurs prior to the stromatolites in the Çürük Dag section (Kershaw et al., 2011), possibly reflecting the difference in palaeoclimatology or palaeogeography between two areas.

Despite the migration of sedimentary facies during the transgression process that leads to variable stratigraphic sequences, other factors, such as terrigenous input, would also have an impact on the development of microbialites. For example, in Xiajiacao and Zuodeng sections, the top of the microbialite is overlain by mud-rich sediments (Fig. 10), indicating that terrigenous input could have also led to the termination of microbialite growth thereby limiting development of the full microbialite sequence.

Because of the complexity of geological processes, our proposed model can, of course, not include all the patterns of different sections. Further detailed analysis of sedimentary sequences from more sections promises to yield evidence that may be used for the more specific identification of palaeogeographical settings and reconstruction of palaeoecological details of the basal Triassic transgression.

5.2 Relationship between $\delta^{13}C$ excursion and the transgression

The sedimentary sequence of microbialites in the Chongyang section records the progress of the transgression at the beginning of Early Triassic. It is interesting to compare this evidence with the evidence provided from the analysis of the contemporaneous variation of carbon isotopes.

The negative excursion of $\delta^{13}C$ value has variously been interpreted to be related to volcanogenic CO_2 input in the oceanic carbon cycle (Korte et al., 2010), leakage and oxygenation of methane hydrate (Kajiwara et al., 1994), or upwelling of anoxic deep seawater (Knoll et al., 1996; Algeo et al., 2007). However, the amount of volcanogenic CO_2 was considered to be insufficient to result in a global oceanic negative excursion of

$\delta^{13}C$ values (Berner, 2002), and there is no substantial evidence yet to support the suggestion of leakage of methane hydrate. By contrast, upwelling of anoxic deep ocean water evidenced by sulfur isotope from both shallow- and deep- water sections (Algeo et al., 2008; Shen et al., 2011) provides a credible alternative explanation for the negative excursion of $\delta^{13}C$ values and the marine biotic extinction (Knoll et al., 1996).

However, the causes of the biotic extinction are likely to have been more complex, and may include the effects of lethally high temperatures (Sun et al, 2012), anoxic events (Kump et al., 2005; Algeo et al., 2007; Korte and Kozur, 2010), volcanism (Yin et al., 1989; Yang et al., 1991; Kamo et al., 2003; Yin and Song, 2013) and significant eustatic fall causing widespread regression (Yin et al., 2014). However, geological records show that all these events seem to have happened simultaneously (Chen and Benton, 2012). Therefore, it is difficult to attribute the biotic mass extinction to a single event or to a particular combination of causes.

Oceanic anoxia has long been considered as an important factor leading to the extinction of benthic organisms in marine facies sequences. The most likely cause of such a negative $\delta^{13}C$ excursion was the upwelling of the deep anoxic water. Yet, the evidence of framboidal pyrite in deep-water sections in South China shows a relatively long oxygenated period in the aftermath of the mass extinction (He et al., 2013; Li et al., 2016). In shallow-water platform environments, although pyrite framboids can usually be found within the microbialites that overly the extinction horizon, statistical analysis of framboid diameters indicate dysoxic environments rather than anoxic conditions across the shallow platforms in South China (Liao et al., 2017). The presence of a rich fauna, including ostracods (Crasquin-Soleau and Kershaw, 2005; Liu et al., 2010), gastropods (Jiang et al., 2010) and brachiopods (this study) provides evidence to support the conclusion that shallow-water environments were oxic enough for the survival of metazoans. Tang et al. (2017) recently proposed that the micrbialites formed in the Early Triassic transgressive sections they studied were apparently unaffected by contemporary deeper shelf anoxia. Nevertheless, this does not entirely rule out the influence of the oceanic upwelling on platform environments. Evidences of the carbon and sulfur isotopic data showing a positive correlation from Nhi Tao section of Vietnam,

one of the isolated shallow platforms in Nanpanjiang Basin on the southern margin of the south China craton (Lehrmann et al., 2003), suggests that there were frequent intrusions of anoxic water onto the shallow platform (Algeo et al., 2007, 2008). One possible explanation for this variation might be rapid degassing of hydrogen sulfide and carbon dioxide produced by the decreasing pressure when deep water rises onto shallow shelf environments.

In many other sections, both from deep-water (Xie et al., 2007; Riccardi et al., 2007) and shallow-water sediments (Luo et al., 2011), the most negative value of $\delta^{13}C$ does not correspond with the horizon of first pulse of main extinction boundary. Clearly the first episodic mass extinction happened before the occurrence of the most negative value of carbon isotope. Given the close relationship between the negative values of carbon isotopes and the intensity of upwelling of anoxic water, it follows that the first episodic mass extinction was unlikely to have been the result of an anoxic event induced by the upwelling of deep marine water at this location, but it is reasonable to suggest that it could explain the later negative excursion of carbon isotopes.

It is interesting that the abundance of metazoans within the microbialite interval of Chongyang section increases simultaneously with both the apparent increase of water depth and the negative excursion of $\delta^{13}C$ value. This implies that low-level of oxygen possibly caused by the upwelling of anoxic deep water did not inhibit the metazoan activities. Instead, a certain degree of water deepening could effectively protect animals from hot temperature (Sun et al., 2012) at least in the shallow carbonate platform environments.

6. Conclusions

A 10-m-thick interval of microbialite-dominated limestone formed during the earliest Triassic transgression on the carbonate platform of Chongyang section. The first microbialites were stratiform stromatolites, followed by tabular thrombolites interbedded with columnar stromatolite, which were, in turn, followed by domical thrombolites, but microbialite formation terminated at the commencement of oolite deposition.

Based on the microfacies and comparison with modern microbialite distributions, it is suggested that the stratiform stromatolites formed in a tranquil, very shallow water environment, while the tabular thrombolites and the succeeding domical thrombolites indicate progressively deeper environments. The occurrence of a bed of columnar stromatolite may indicate temporary shallowing or restriction. The beginning of oolitic deposition reflects deepening of water depth and changed hydrodynamics, factors that were also responsible for the disappearance of microbialites. We conclude that the microbialite succession records the progress of sea-level rise during the early stages of the transgression.

Increase of water depth effectively protected the residual metazoans from high temperature, but the gradual increase in metazoans eventually resulted in increasing ecosystem complexity that led to the transition from stromatolites to thrombolites.

In the Chongyang section, the first pulse of mass extinction was obviously earlier than the time of the most negative carbon isotope values. Therefore, upwelling of anoxic deep ocean water is unlikely to have been the cause of the first pulse of the mass extinction, though it can reasonably explain the negative excursion of $\delta^{13}C$ value. However, the end-Permian extensive regression that led to the exposure of most shallow-water platforms provides a plausible explanation for the first episodic eclipse of shallow-water benthos.

Acknowledgments

We thank Thomas Algeo for his helpful suggestions that have led to significant improvements to the paper. Steve Kershaw and another anonymous reviewer are appreciated for their valuable comments. This study was jointly supported by the National Natural Science Foundation of China (Grants No.41730320 and No. 41572001) and the 111 project (B08030).

References

Adachi, N., Asada, Y., Ezaki, Y., Liu, J., 2017. Stromatolites near the Permian–Triassic boundary in Chongyang, Hubei Province, South China: A geobiological window into palaeo-oceanic fluctuations following the end-Permian extinction. Paleogeogr. Paleoclimatol. Paleoecol. 475, 55-69

Algeo, T.J., Ellwood. B., Nguyen, T.K.T., Rowe, H., Maynard, J.B., 2007. The Permian–Triassic boundary at Nhi Tao, Vietnam: evidence for recurrent influx of sulfidic watermasses to a shallow-marine carbonate platform. Paleogeogr. Paleoclimatol. Paleoecol. 252, 307–327.

Algeo, T.J., Shen, Y., Zhang, T., Lyons, T., Bates, S., Rowe, H., Nguyen, T.K.T., 2008. Association of ^{34}S-depleted pyrite layers with negative carbonate δ^{13}C excursions at the Permian-Triassic boundary: Evidence for upwelling of sulfidic deep-ocean water masses. Geochem. Geophys. Geosyst. 9, Q04025, doi:10.1029/2007GC001823.

Algeo, T.J., Chen, Z., Fraiser, M.L., Twitchett, R.J., 2011. Terrestrial-marine teleconnections in the collapse and rebuilding of Early Triassic marine ecosystems. Paleogeogr. Paleoclimatol. Paleoecol. 308, 1–11.

Batchelor, M.T., Burne, R.V., Hery, B.L., Li, F., Paul, J., 2017. A biofilm and organo-mineralisation model for the growth and limiting size of ooids. Sci. Rep. (in press).

Baud, A., Richoz, S., Pruss, S., 2007. The lower Triassic anachronistic carbonate facies in space and time. Glob. Planet. Change. 55: 81–89.

Berner, R.A., 2002. Examination of hypotheses for the Permo-Triassic boundary extinction by carbon cycle modeling. Proc. Natl. Acad. Sci. 99, 4172–4177.

Bosak, T., Knoll, A.H., Petroff, A.P., 2013. The meaning of stromatolites. Annu. Rev. Earth Planet. Sci. 41: 21–44.

Burne, R.V., Johnson, K., 2012. Sea-level variation and the zonation of microbialites in Hamelin Pool, Shark Bay, Western Australia. Mar. Freshw. Res. 63, 994–1004.

Chen Z.Q., Benton M.J., 2012. The timing and pattern of biotic recovery following the end-Permian mass extinction. Nat. Geosci. 5, 375–383.

Crasquin-Soleau, S., Kershaw, S., 2005. Ostracod fauna from the Permian-Triassic boundary interval of South China (Huaying Mountains, eastern Sichuan Province): palaeoenvironmental significance. Paleogeogr. Paleoclimatol. Paleoecol. 217, 131–141.

Deng, B., Wang, Y., Woods, A., Li, S., Li, G., Chen, W., 2017. Evidence for rapid precipitation of calcium carbonate in South China at the beginning of Early Triassic. Paleogeogr. Paleoclimatol. Paleoecol. 474, 187–97.

Diaz, M.R., Swart, P.K., Eberli, G.P., Oehlert, A.M., Devlin, Q., Saeid, A., Altabet, M.A., 2015. Geochemical evidence of microbial activity within ooids. Sedimentology. 62, 2090–2112.

Dill, R.F., Shinn, E.A., Jones, A.T., Kelly, K. Steinen, R.P., 1986. Giant subtidal stromatolites forming in normal salinity waters. Nature, 324, 55–58.

Ezaki, Y., Liu, J., Adachi, N., 2003. Earliest Triassic microbialite micro-to megastructures in the Huaying area of Sichuan Province, South China: implications for the nature of oceanic conditions after the end-Permian extinction. Palaios.18, 388–402.

Fan, J., Yang, W., Wen, C., Rui, L., Lu, L., Wang, K., Mu, X., Permian reefs in Laolongdong of Beipei of Chongqing. In Fan eds: The ancient organic reefs of China and their relations to oil and gas. Marine Press, Beijing, pp. 170–244 (in Chinese).

Fang, Y., Chen, Z., Kershaw, S., Yang, H., Luo, M., 2017. Permian-Triassic boundary microbialites at Zuodeng Section, Guangxi Province, South China: Geobiology and palaeoceanographic implications. Glob. Planet. Change. 152, 115–128.

Farabegoli, E., Perri, M.C., 2012. Millennial physical events and the end-Permian mass mortality in the western Palaeotethys: timing and primary causes. Earth and Life. Springer, Netherlands, pp. 719–758.

Feldmann, M., McKenzie, J., 1998. Stromatolite-thrombolite associations in modern environment, Lee Stocking Island, Bahamas. Palaios.13, 201–212.

Feng, Z., Bao, Z., Li, S., 1997. Lithofacies palaeogeography of the early and Middle Triassic of south China. Sci. Geol. Sin. 32, 212–220.

Garrett, P., 1970. Phanerozoic stromatolites: non-competative ecology restriction by grazing and burrowing animals. Science. 169, 171–173.

Gleeson, D.B., Wacey, D., Waite, I., O'Donnell, A.G., Kilburn, M.R., 2016. Biodiversity of living, non-marine, thrombolites of Lake Clifton, Western Australia. Geomicrobiol. J. 33, 850–859.

Golubic, S., 1991. Modern stromatolites: a review//Calcareous algae and stromatolites. Springer Berlin Heidelberg. 545.

Glumac, B., Walker, K.R., 1997. Selective dolomitization of Cambrian microbial carbonate deposits: a key to mechanisms and environments of origin. Palaios. 12, 98–110.

He, L., Wang, Y., Woods, A., Li, G., Yang, H., Liao, W., 2013. An oxygenation event occurred in deep shelf settings immediately after the end-Permian mass extinction in South China. Glob. Planet. Change. 101, 72–81.

Heydari, E., Hassanzadeh, J., Wade, W.J., Ghazi, A.M., 2003. Permian-Triassic boundary interval in the Abadeh section of Iran with implications for mass extinction: Part 1–Sedimentology. Paleogeogr. Paleoclimatol. Paleoecol. 193, 405–423.

Jahnert, R.J., Collins, L.B., 2013. Controls on microbial activity and tidal flat evolution in Shark Bay, Western Australia. Sedimentology. 60, 1071–1099.

Jiang, H., Lai, X., Sun, Y., Wignall, P.B., Liu, J., Yan, C., 2014. Permian-Triassic conodonts from Dajiang (Guizhou, South China) and their implication for the age of microbialite deposition in the aftermath of the end-Permian mass extinction. J. Earth Sci. 25, 413–430.

Jiang, H., Wu, Y., Diao, J., Chen, J., 2010. A Dwarf Euomphalid fauna from the Permian-Triassic boundary in Laolongdong, Beibei, Chongqing: opportunity taxa surviving the disaster event?. Acta Geoscientica Sinica. 31, 163–169. (In Chinese with English abstract)

Kajiwara, Y., Yamakita, S., Ishida, K., Ishiga, H., Imai, A., 1994. Development of a largely anoxic stratified ocean and its temporary massive mixing at the

Permian/Triassic boundary supported by the sulfur isotopic record. Paleogeogr. Paleoclimatol. Paleoecol. 111, 367–379.

Kershaw, S., Zhang, T., Lan, G., 1999. A? microbialite carbonate crust at the Permian-Triassic boundary in South China, and its palaeoenvironmental significance. Paleogeogr. Paleoclimatol. Paleoecol. 146, 1–18.

Kershaw, S., Li, Y., Crasquin-Soleau, S., Feng, Q., Mu, X., Collin, P., Reynolds, A., Guo, L., 2007. Earliest Triassic microbialites in the South China block and other areas: controls on their growth and distribution. Facies. 53, 409–425.

Kershaw, S., Crasquin, S., Forel, M-B., Randon, C., Collin, P-Y., Kosun, E., Richoz, S., Baud, A., 2011. Earliest Triassic microbialites in Çürük Dag, southern Turkey: composition, sequences and controls on formation. Sedimentology. 58, 739–755.

Kershaw, S., Crasquin, S., Li, Y., Collin, P., Forel, M., Mu, X., Baud, A., Wang, Y., Xie, S., Maurer, F., Guo, L., 2012. Microbialites and global environmental change across the Permian–Triassic boundary: a synthesis. Geobiology. 10, 25–47.

Knoll, A.H., Bambach, R.K., Canfield, D.E., Grotzinger, J.P., 1996. Comparative Earth history and late Permain mass extinction. Science. 273, 452.

Kamo, S.L., Czamanske, G.K., Amelin, Y., Fedorenko, V.A., Davis, D.W., Trofimov V.R., 2003. Rapid eruption of Siberian flood-volcanic rocks and evidence for coincidence with the Permian-Triassic boundary and mass extinction at 251Ma. Earth Planet. Sci. Lett. 214, 75–91.

Korte, C., Kozur, H.W., 2010. Carbon-isotope stratigraphy across the Permian-Triassic boundary: a review. J. Asian Earth Sci. 39, 215–235.

Korte, C., Pande, P., Kalia, P., Kozur, H.W., Joachimski, M.M., Oberhänsli, H., 2010. Massive volcanism at the Permian-Triassic boundary and its impact on the isotopic composition of the ocean and atmosphere. J. Asian Earth Sci. 37, 293–311.

Kump, L.R., Pavlov, A., Arthur, M.A., 2005. Massive release of hydrogen sulfide to the surface ocean and atmosphere during intervals of oceanic anoxia. Geology. 33, 397–400.

Lehrmann, D.J., 1999. Early Triassic calcimicrobial mounds and biostromes of the Nanpanjiang basin, south China. Geology. 27, 359–362.

Lehrmann, D.J., Payne, J.L., Felix, S.V., Dillett, P.M., Yu, Y., Wei, J., 2003. Permian-Triassic boundary sections from shallow-marine carbonate platforms of the Nanpanjiang Basin, South China: implications for oceanic conditions associated with the end-Permian extinction and its aftermath. Palaios. 18, 138–152.

Li, F., Yan, J., Burne, R.V., Chen, Z-Q., Algeo, T.J., Zhang, W., Tian, L., Gan, Y., Xie, S., 2017. Palaeo-seawater REE compositions and microbial signatures preserved in laminae of Lower Triassic ooids. Paleogeogr. Paleoclimatol. Paleoecol. 486, 96–107.

Li, G., Wang, Y., Shi, G., Liao, W., Yu, L., 2016. Fluctuations of redox conditions across the Permian-Triassic boundary—New evidence from the GSSP section in Meishan of South China. Paleogeogr. Paleoclimatol. Paleoecol. 448, 48–58.

Liao, W., Bond, D., Wang, Y., He, L., Yang, H., Weng, Z., Li G., 2017. An extensive anoxic event in the Triassic of the South China Block: a pyrite framboid study from Dajiang and its implications for the cause(s) of oxygen depletion. Paleogeogr. Paleoclimatol. Paleoecol. 486, 86–95.

Liu, H., Wang, Y., Yuan, A., Yang, H., Song, H., Zhang, S., 2010. Ostracod fauna across the Permian-Triassic boundary at Chongyang, Hubei Province, and its implication for the process of the mass extinction. Sci. China Earth Sci. 53, 810–817.

Liu, J., Ezaki, Y., Yang, S., Wang, H., Adachi, N., 2007. Age and sedimentology of microbialites after the end-Permian mass extinction in Luodian, Guizhou Province. J. Paleogeogr. 9, 473–486. (In Chinese with English abstract).

Loreau, J.P., Purser, B.H., 1973. Distribution and ultrastructure of Holocene ooids in the Persian Gulf. The Persian Gulf. Springer, Berlin Heidelberg, pp. 279–328.

Luo, G., Kump, L.R., Wang, Y., Tong, J., Arthur, M.A., Yang, H., Huang, J., Yin, H., Xie, S., 2010. Isotopic evidence for an anomalously low oceanic sulphate concentration following end-Permian mass extinction. Earth Planet. Sci. Lett. 300, 101–111.

Luo, G., Wang, Y., Yang, H., Algeo, T., Kump, L., Huang, J., Xie, S., 2011. Stepwise and large-magnitude negative shift in $\delta^{13}C_{carb}$ preceded the main marine mass extinction of the Permian-Triassic crisis interval. Paleogeogr. Paleoclimatol. Paleoecol. 299, 70–82.

Luo, H., Zhou, Z., Cai, H., Zhu, Y., Wang, Z., Chen, J., Xu, B., Yang, H., Chen, H., Chen, D., 2013. Permian-Triassic boundary biostratigraphy and sedimentology at the Yudongzi section of Jiangyou, Sichuan Province. J. Stratigr. 37, 81–92 (in Chinese, with English abstract).

McCrea, J.M., 1950. The isotopic chemistry of carbonates and a paleotemperature scale. J. Chem. Phys., 18, 849–857.

Monty, C.L.V., 1976. The origin and development of cryptalgal fabrics., in M.R. Walter (editor) Stromatolites, developments in sedimentology, 20, pp. 193–249.

Moore, L.S., Burne, R.V., 1994. The modern thrombolites of Lake Clifton, western Australia. In Phanerozoic stromatolites II (pp. 3–29). Springer Netherlands.

Newell, N.D., 1967. Revolutions in the history of life. Geol. Soc. Am., Spec. Pap. 89, 63–91.

Nutman, A.P., Bennett, V.C., Friend, C.R.L., Kranendonk, M.J.V., Chivas, A.R., 2016. Rapid emergence of life shown by discovery of 3,700-million-year-old microbial structures. Nature. 537, 535–538.

O'reilly, S.S., Mariotti, G., Winter, A.R., Newman, S.A., Matys, E.D., McDermott, F., Pruss, S.B., Bosak, T., Summons, R.E. Klepac-Ceraj, V., 2017. Molecular biosignatures reveal common benthic microbial sources of organic matter in ooids and grapestones from Pigeon Cay, The Bahamas. Geobiology. 15, 112–130.

Pei, Y., Chen, Z., Fang, Y., Kershaw, S., Wu, S., Luo, M., 2017. Volcanism, redox conditions, and microbialite growth linked with the end-Permian mass

extinction: Evidence from the Xiajiacao section (western Hubei Province), South China. Palaeogeogr. Palaeoclimatol. Palaeoecol. (in press).

Planavsky, N., Ginsburg, R.N., 2009. Taphonomy of modern marine Bahamian microbialites. Palaios. 24, 5–17.

Pratt, B.R., 1984. Epiphyton and Renalcis-diagenetic microfossils from calcification of coccoid blue-green algae. J. Sediment. Petrol. 54, 948–971.

Riccardi, A., Kump, L.R., Arthur, M.A., D'Hondt, S., 2007. Carbon isotopic evidence for chemocline upward excursions during the end-Permian event. Paleogeogr. Paleoclimatol. Paleoecol. 248, 73–81.

Shen, Y., James, F., Zhang, H., Andrew, M., Zhang, T., Boswell, A.W., 2011. Multiple S-isotopic evidence for episodic shoaling of anoxic water during Late Permian mass extinction. Nat. Commun. 2, 210–214.

Sun, Y., Joachimski, M.M., Wignall, P.B., Yan, C., Chen, Y., Jiang, H., Wang, L., Lai, X., 2012. Lethally hot temperatures during the Early Triassic greenhouse. Science. 338, 366–370.

Suosaari, E.P., Reid, R.P., Playford, P.E., Foster, J.S., Stolz, J.F., Casaburi, G., Hagan, P.D., Chirayath, V.I., Macintyre, G.N., Planavsky, J., Eberli, G.P., 2016. New multi-scale perspectives on the stromatolites of Shark Bay, Western Australia. Sci. Rep. 6, 20557.

Tang, H., Kershaw, S., Liu, H., Tan, X., Li, F., Hu, G., Huang, C., Wang, L., Lian, C., Li, L., Yang, X., 2017. Permian–Triassic boundary microbialites (PTBMs) in southwest China: implications for paleoenvironment reconstruction. Facies, 63:2, 23pages.

Theisen, C.H., Sumner, D.Y., 2016. Thrombolite fabrics and origins: influences of diverse microbial and metazoan processes on Cambrian thrombolite variability in the Great Basin, California and Nevada. Sedimentology. 63, 2217–2252.

Walter, M.R., Heys, G.R., 1985. Links between the rise of Metazoa and the decline of stromatolite. Precambrian Res. 29, 149–174.

Wang, L., Wignall, P.B., Wang, Y., Jiang, H., Sun, Y., Li, G., Yuan, J., Lai, X., 2016. Depositional conditions and revised age of the Permo-Triassic microbialites at

Gaohua section, Cili County (Hunan Province, South China). Paleogeogr. Paleoclimatol. Paleoecol. 443, 156–166.

Wang, S., Qiang, Z., Wen, Y., Tao, Y., 1994. Petrology and origin of the calcareous crusts capping the Permian reefs in Huaying Mountains, Sichuan. J. Miner. Petrol. 14, 59–68 (in Chinese, with English abstract).

Wang, Y., Tong, J., Wang, J., Zhou, X., 2005. Calcimicrobialite after end-Permian mass extinction in South China and its palaeoenvironmental significance. Chin. Sci. Bull. 50, 665–671.

Wu, S., Chen, Z., Fang, Y., Pei, Y., Yang, H., Ogg, J., 2017. A Permian-Triassic boundary microbialite deposit from the eastern Yangtze Platform (Jiangxi Province, South China): Geobiologic features, ecosystem composition and redox conditions. Paleogeogr. Paleoclimatol. Paleoecol. 486, 58–73.

Wu, Y., Fan, J., Jin, Y., 2003. Emergence of the Late Permian changhsingian reefs at the end of the Permian. Acta Geologica Sci. 77, 289–296.

Wu, Y., Jiang, H., Yang, W., Fan, J., 2007. Microbialite of anoxic condition from Permian-Triassic transition in Guizhou, China. Sci. China Ser. D-Earth Sci. 50, 1040–1051.

Wu, Y., Jiang, H., Fan, J., 2010. Evidence for sea-level falls in the Permian-Triassic transition in the Ziyun area, South China. Geol. J. 45, 170–185.

Wu, Y., Yu, G., Li, R., Song, Li., Jiang, H., Riding, R., Liu, L., Liu, D., Zhao, R., 2014. Cyanobacterial fossils from 252 Ma old microbialites and their environmental significance. Sci. Rep. 4, 3820.

Wu, Y., Yu, G., Jiang, H., Liu, L., Zhao, R., 2016. Role and lifestyle of calcified cyanobacteria (Stanieria) in Permian-Triassic boundary microbialites. Paleogeogr. Paleoclimatol. Paleoecol. 448, 39–47.

Xie, S., Pancost, R.D., Huang, J., Wignall, P.B., Yu, J., Tang, X., Chen, L., Huang, X., Lai, X., 2007. Changes in the global carbon cycle occurred as two episodes during the Permian-Triassic crisis. Geology. 35, 1083–1086

Xie, S., Algeo, T.J., Zhou, W., Ruan, X., Luo, G., Huang, J., Yan, J., 2017. Contrasting microbial community changes during mass extinctions at the Middle/Late

Permian and Permian/Triassic boundaries. Earth Planet. Sci. Lett. 460, 180–191.

Xu, G., Luo, X., Wang, Y., Zhou, L., Xiao, S., 1997. On a building model of Late Permian reefs in central Yangtze River area. China University of Geosciences Press, Wuhan, pp. 67–71 (in Chinese, with English abstract).

Yang, H., Chen, Z., Wang, Y., Tong, J., Song, H., Chen, J., 2011. Composition and structure of microbialite ecosystems following the end-Permian mass extinction in South China. Paleogeogr. Paleoclimatol. Paleoecol. 308, 111–128.

Yang, Z., Wu, S., Yin, H., Xu, G., Zhang, K., Bi, X., 1991. Permo-Triassic events of South China. Geological Publishing House, Beijing, pp. 3–138 (in Chinese, with English abstract).

Yin, H., Huang, S., Zhang, K., Yang, F., Ding, M., Bi, X., Zhang, S., 1989. Volcanism at the Permian-Triassic boundary in South China and its effects on mass extinction. Acta Geol. Sin. 63, 169–180. (In Chinese with English abstract)

Yin, H., Zhang, K., Tong, J., Yang, Z., Wu, S., 2001. The global stratotype section and point (GSSP) of the Permian-Triassic boundary. Episodes. 24, 102–114.

Yin, H., Song, H., 2013. Mass extinction and Pangea integration during the Paleozoic-Mesozoic transition. Sci. China-Earth Sci. 56, 1791–1803.

Yin, H., Jiang, H., Xia, W., Feng, Q., Zhang, N., Shen, J., 2014. The end-Permian regression in South China and its implication on mass extinction. Earth-Sci. Rev. 137, 19–33.

Zhang, W., Shi, X., Tang, D., Wang, X., 2016. The characteristic and genetic interpretation of thrombolite in Mesoproterozoic Gaoyuzhuang Formation from Pingquan, Hebei Province. Chin. J. Geol. 51, 1324–1343 (in Chinese, with English abstract).

Zhu, S., Liang, Y., Du, R., 1993. The Stromatolites of China. Tianjin University Press, Tianjin, pp. 191–196 (in Chinese, with English abstract).

Table 1

Carbon and oxygen isotopic data listed with rock types and sampling levels in Chongyang section.

Meter level	Rock type	$\delta^{13}C_{PDB}$ (‰)	$\delta^{18}O_{VPDB}$ (‰)	Meter level	Rock type	$\delta^{13}C_{PDB}$ (‰)	$\delta^{18}O_{VPDB}$ (‰)
914.0	Oolite	-0.0671	-8.0578	228.5	Microbialite	-0.1601	-7.4093
848.5	Oolite	0.1735	-8.1339	219.5	Microbialite	0.6965	-6.7778
833.5	Oolite	0.2841	-6.503	203.0	Microbialite	0.5994	-6.8209
793.0	Oolite	-0.1834	-8.6735	187.5	Microbialite	0.9245	-5.8047
761.0	Oolite	-0.0473	-6.9509	166.5	Microbialite	0.6451	-6.5495
724.0	Oolite	-0.1237	-7.5744	156.5	Microbialite	0.5968	-7.1784
662.5	Microbialite	-0.0929	-7.4272	143.0	Microbialite	0.7779	-8.9717
620.5	Microbialite	0.3403	-8.5441	136.0	Microbialite	1.0958	-8.6417
599.0	Microbialite	0.1216	-7.136	119.0	Microbialite	1.0442	-8.4562
580.0	Microbialite	0.0045	-7.2875	102.0	Microbialite	1.2298	-8.2946
571.0	Microbialite	-0.1254	-9.1166	81.0	Microbialite	1.6455	-7.6948
541.0	Microbialite	-0.0476	-6.2704	70.0	Microbialite	1.4753	-8.215
523.5	Microbialite	0.0276	-8.6807	59.0	Microbialite	1.3832	-7.8503
500.5	Microbialite	0.0686	-7.4659	45.0	Microbialite	1.5197	-8.3625
482.0	Microbialite	0.1952	-8.4199	25.0	Microbialite	1.3708	-8.351
464.5	Microbialite	-0.0751	-8.4105	15.0	Microbialite	1.4193	-8.4257
440.0	Microbialite	-0.0869	-9.4724	7.5	Microbialite	2.1859	-7.1373
418.5	Microbialite	-0.1133	-8.1064	2.5	Microbialite	1.3611	-8.3173
406.5	Microbialite	-0.0274	-7.9049	-3.5	Bioclastic limestone	1.764	-9.5189
389.0	Microbialite	0.012	-8.0521	-15.5	Bioclastic limestone	2.2756	-8.8825
373.0	Microbialite	0.3772	-7.3889	-30.0	Bioclastic limestone	2.4585	-8.2654
360.5	Microbialite	-0.0913	-8.2138	-39.0	Bioclastic limestone	2.2033	-8.5423
326.0	Microbialite	-0.634	-7.2846	-56.5	Bioclastic limestone	2.6656	-8.2772
301.0	Microbialite	0.2945	-7.1927	-67.5	Bioclastic limestone	2.5284	-8.56
275.0	Microbialite	0.4165	-6.9456	-76.0	Bioclastic limestone	2.331	-8.802
265.5	Microbialite	-0.5362	-6.5433	-95.0	Bioclastic limestone	2.3577	-8.7419
248.0	Microbialite	0.7122	-5.9016	-111.0	Bioclastic limestone	2.763	-7.3014

Figure captions

Figure 1 Early Triassic paleogeography of the South China (modified from Feng et al., 1997).

Figure 2 The lower part of the microbialite interval near the Permian and Triassic boundary in Chongyang section.

Figure 3 The sedimentary sequence and the change of microbialite forms accompanying sea-level fluctuation at the beginning of Early Triassic in Chongyang section. This strata succession clearly reveals increasing biodiversity of marine animals with the deepening of sea water. However, carbon isotopic values exhibit negative correlation with the sea-level change.

Figure 4 Stratiform stromatolites overlying the erosion boundary at Chongyang section. A. Stratiform stromatolite. B. Chambered cyanobacteria in the stratiform stromatolite under the scanning electron microscope. C. Chambered cyanobacteria in the thin section.

Figure 5 The fabric of Early Triassic tabular thrombolite in Chongyang section. M. Micrite patches. S. Sparry clots. The yellow arrows point to ostracods.

Figure 6 Early Triassic columnar stromatolite in Chongyang section. A. Polished section of columnar stromatolite. B. Spherical cyanobacteria within the columnar stromatolite in the thin section. C. Spherical cyanobacteria under the scanning electron microscope.

Figure 7 Domical thrombolites and the bioclastic-enriched sediments filling in the interspace. A. Outcrop of vertical cross sections of large thrombolite domes in the field. DM refers to domical thrombolites, BS refers to bioclastic sediments as the interspace fillings. B. The plane view of the domical thrombolites at an equivalent horizon in a nearby section. C. Bioclastic fillings rich in brachiopods and gastropods.

Figure 8 The oolite overlying the domical thrombolites in Chongyang section. A. Poorly-sorted ooids, field photo. B. Oolites under the microscope, the yellow arrows point to the gastropod fossils as the nucleus of ooids.

Figure 9 Depositional model of the microbialite forms change with the sea-level rise in Early Triassic. At the very beginning of the transgression, stratiform stromatolite firstly formed. With the sea-level rise, tabular thrombolite began to develop. As the further deepening of water, domical thrombolite becomes to dominate but terminated from the deposition of oolites.

Figure 10 Different microbialite sequence and thickness preserved in different palaeogeographic locations during the Early Triassic transgression that followed the end-Permian mass extinction. Section Xiajiacao and section Zuodeng were redrawn from Pei et al. (2017) and Fang et al. (2017) respectively, but with new legends.

Highlights of this paper:

Stromatolites changed into thrombolites during Early Triassic transgression.

Moderate sea-level rise favors the diversification of marine animals.

Enhanced metazoan predation has a marked impact on the fabric of microbialites.

Carbon isotopic value exhibits negative correlation with the depth of sea water.

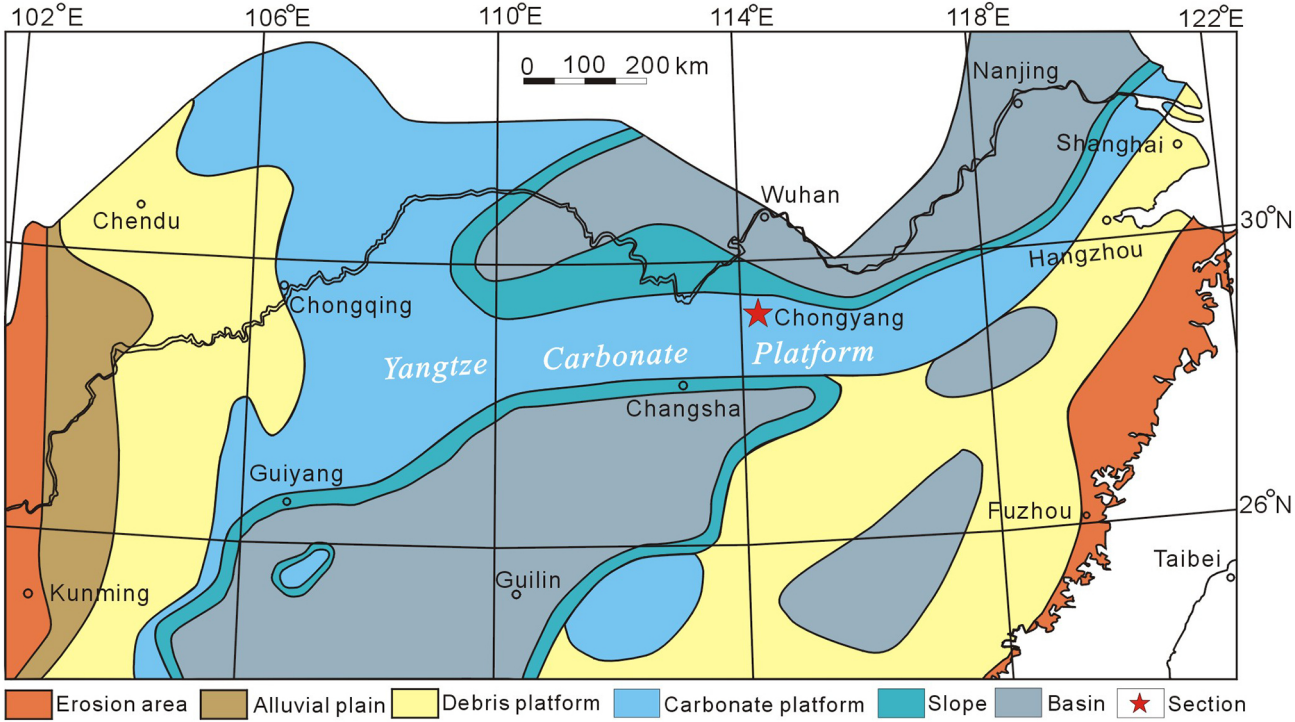
102°E
106°E
110°E
114°E
118°E
122°E
30°N
26°N
0 100 200 km
Nanjing
Shanghai
Wuhan
Chendu
Hangzhou
Chongqing
Chongyang
Yangtze
Carbonate
Platform
Changsha
Guiyang
Fuzhou
Taibei
Kunming
Guilin
Erosion area
Alluvial plain
Debris platform
Carbonate platform
Slope
Basin
Section

Figure 1

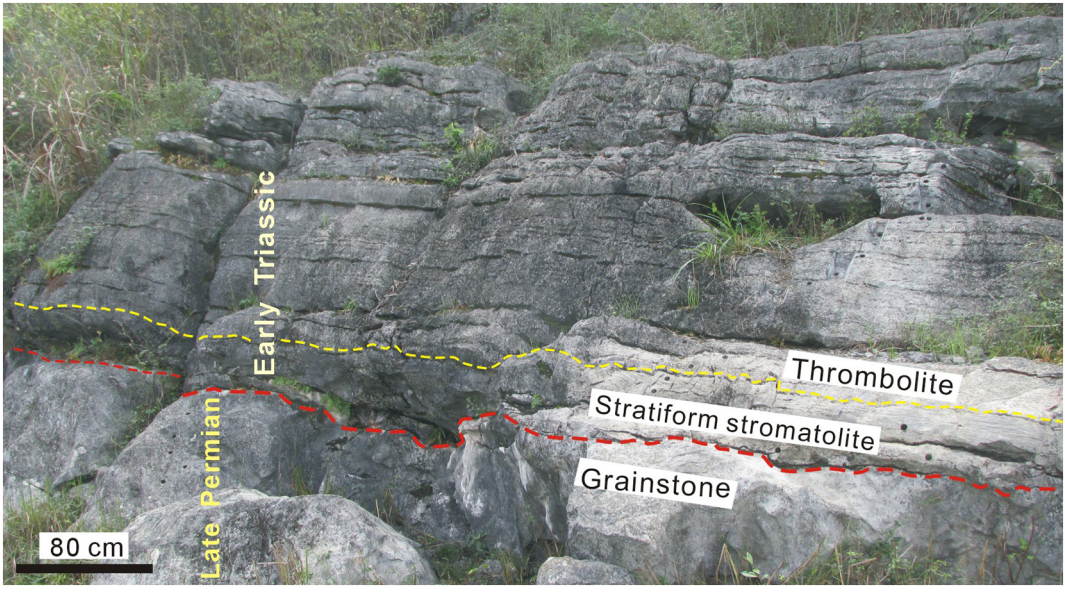
Early Triassic
Late Permian
Thrombolite
Stratiform stromatolite
Grainstone
80 cm

Figure 2

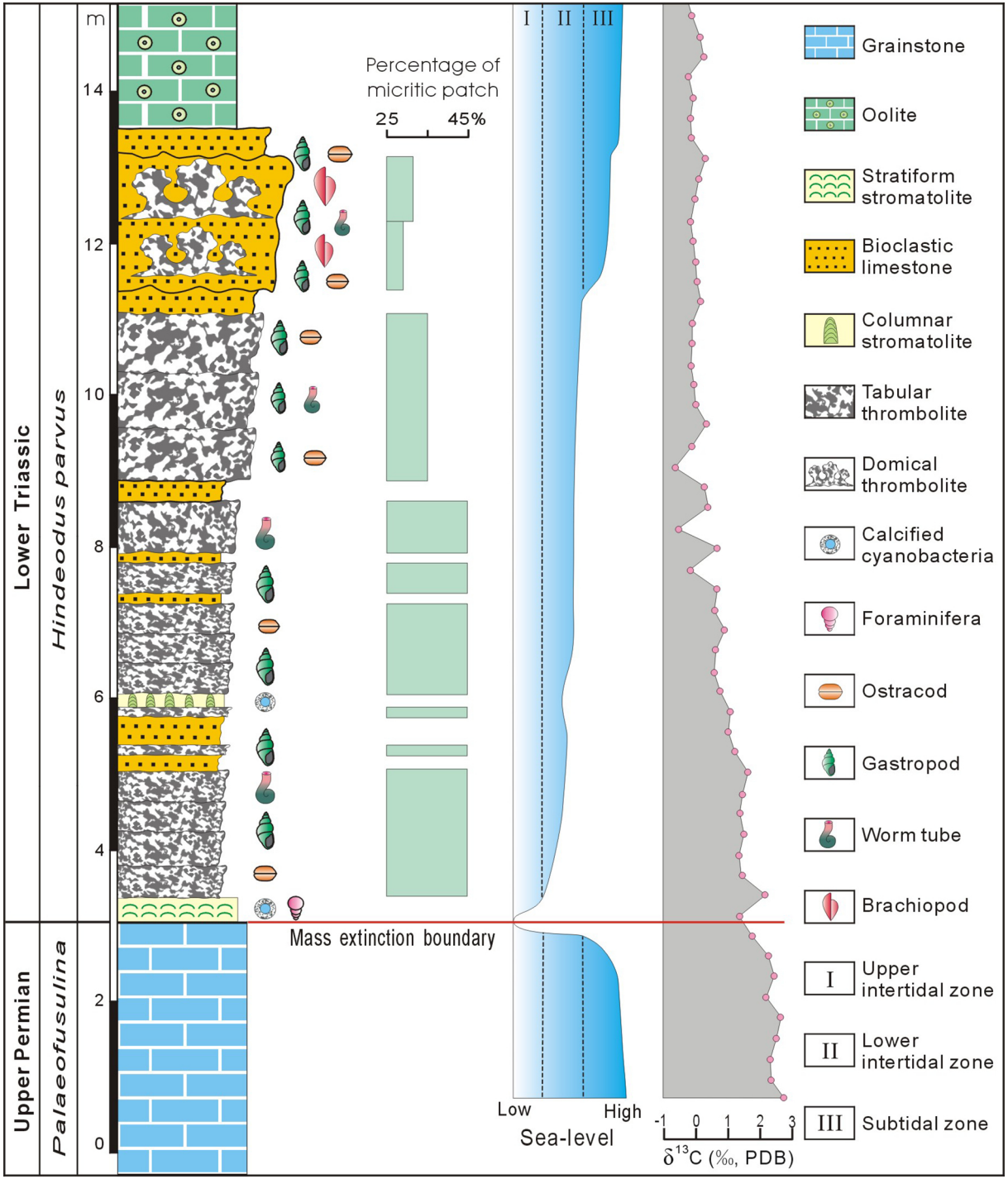
Lower Triassic
Upper Permian
Hindeodus parvus
Palaeofusulina
m
14
12
10
8
6
4
2
0
Percentage of micritic patch
25
45%
Mass extinction boundary
I
II
III
Low
High
Sea-level
-1
0
1
2
3
δ13C (‰, PDB)
Grainstone
Oolite
Stratiform stromatolite
Bioclastic limestone
Columnar stromatolite
Tabular thrombolite
Domical thrombolite
Calcified cyanobacteria
Foraminifera
Ostracod
Gastropod
Worm tube
Brachiopod
I Upper intertidal zone
II Lower intertidal zone
III Subtidal zone

Figure 3

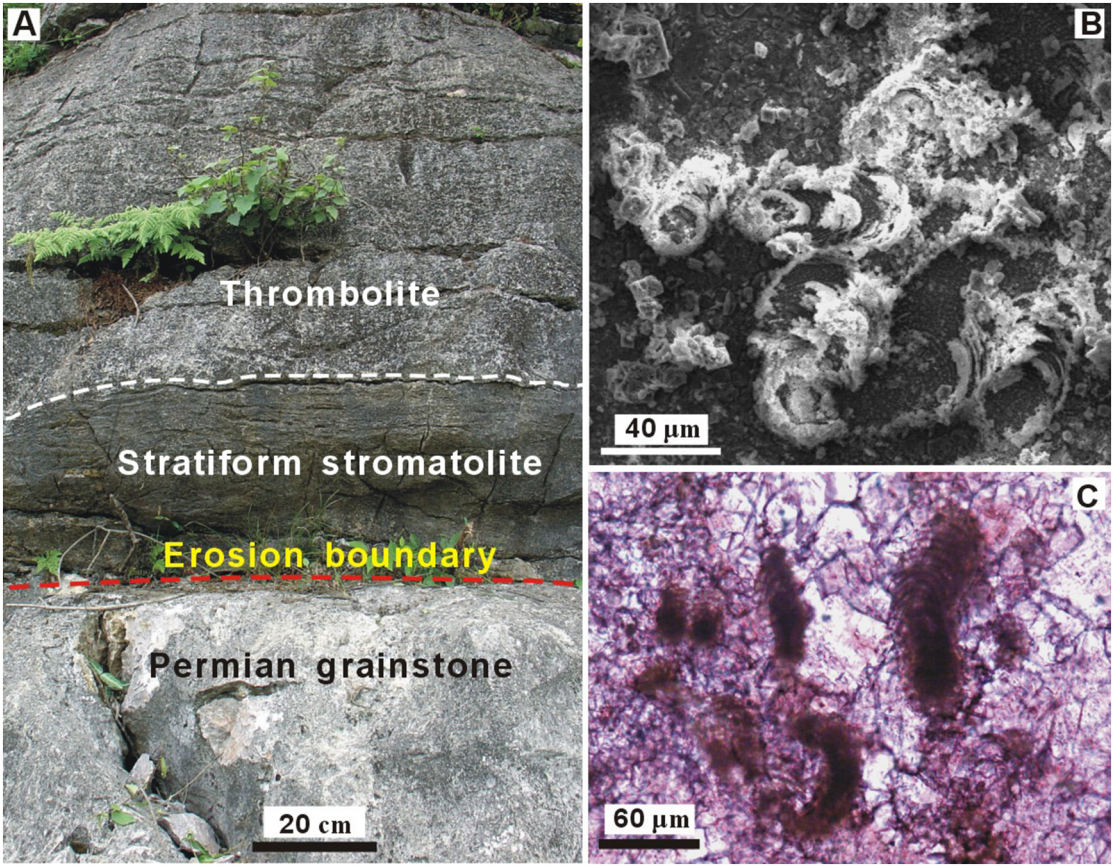
A
Thrombolite
Stratiform stromatolite
Erosion boundary
Permian grainstone
20 cm
B
40 µm
C
60 µm

Figure 4

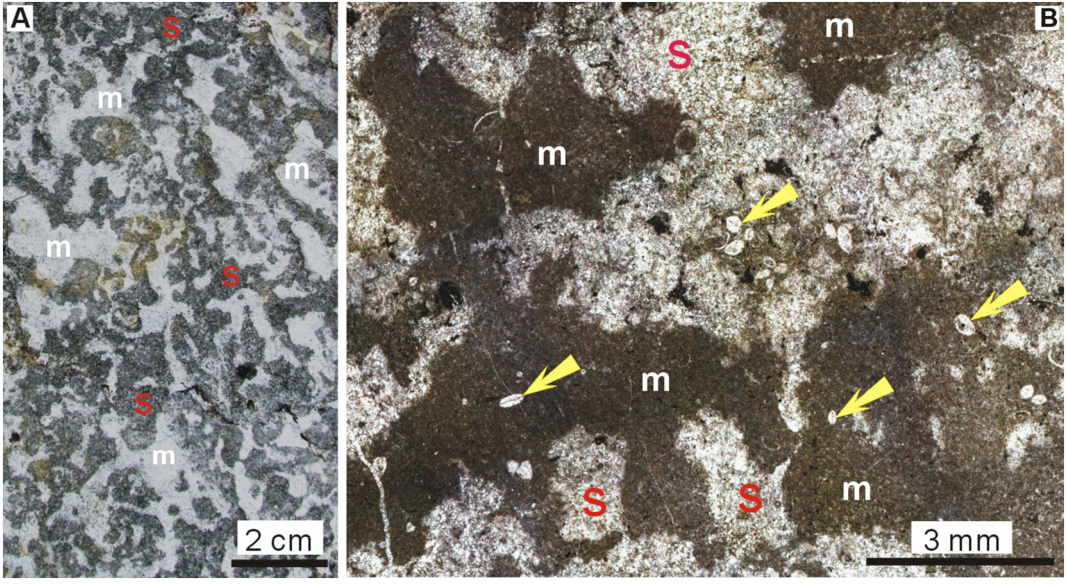

Figure 5

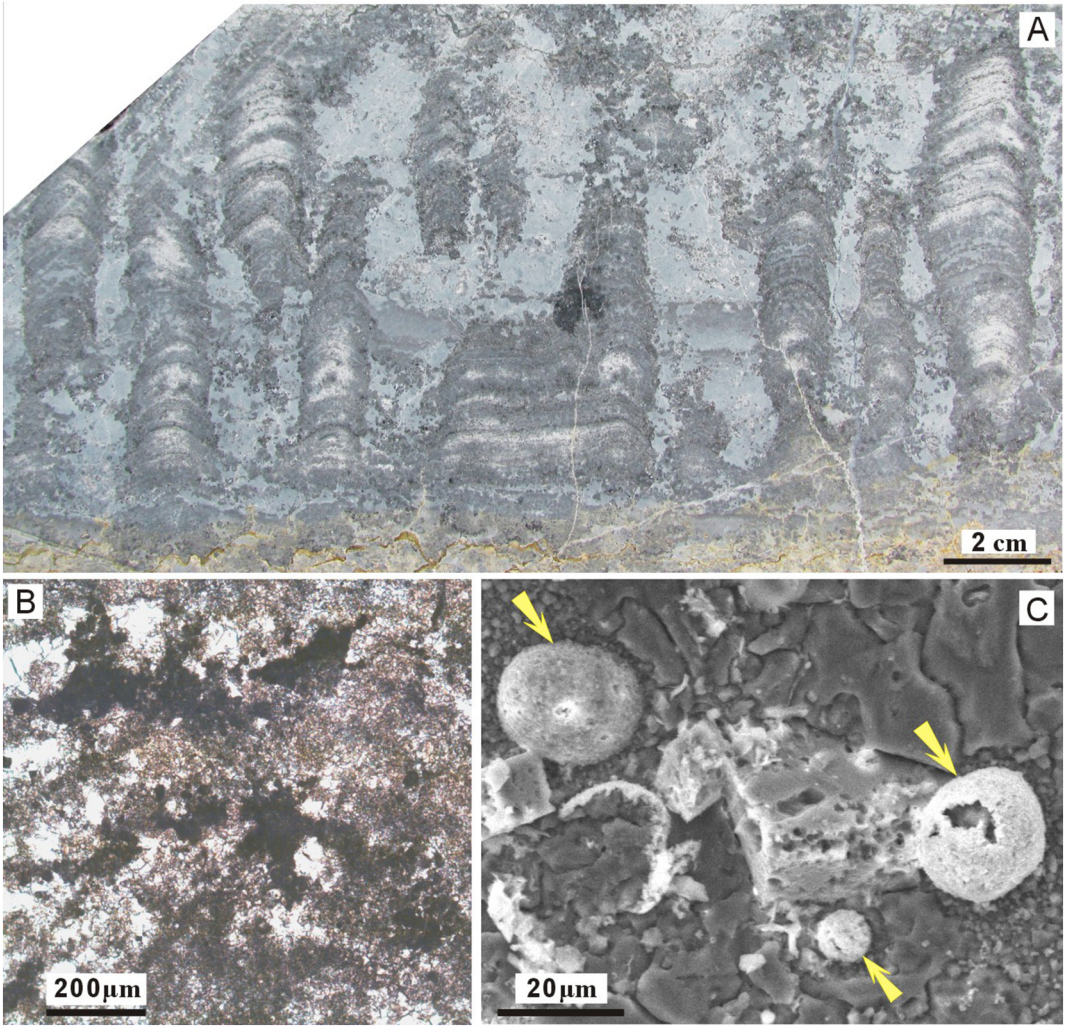

Figure 6

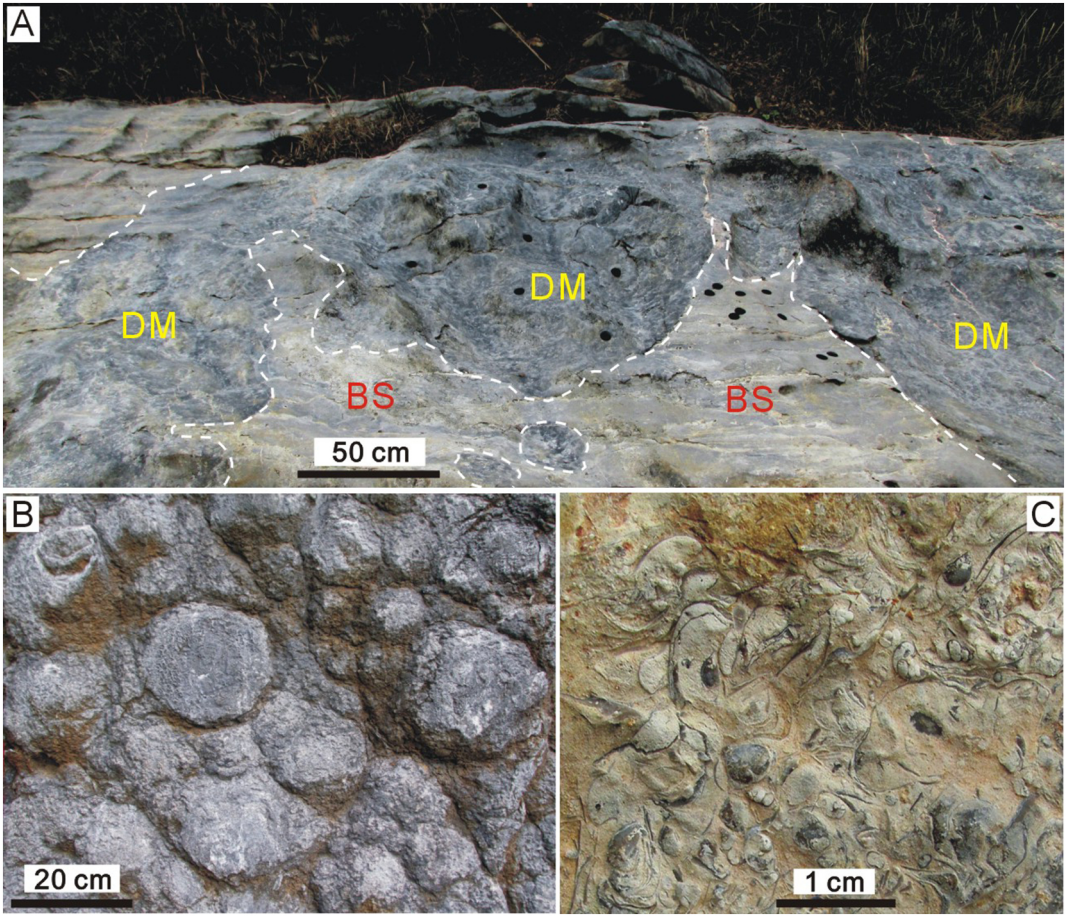

Figure 7

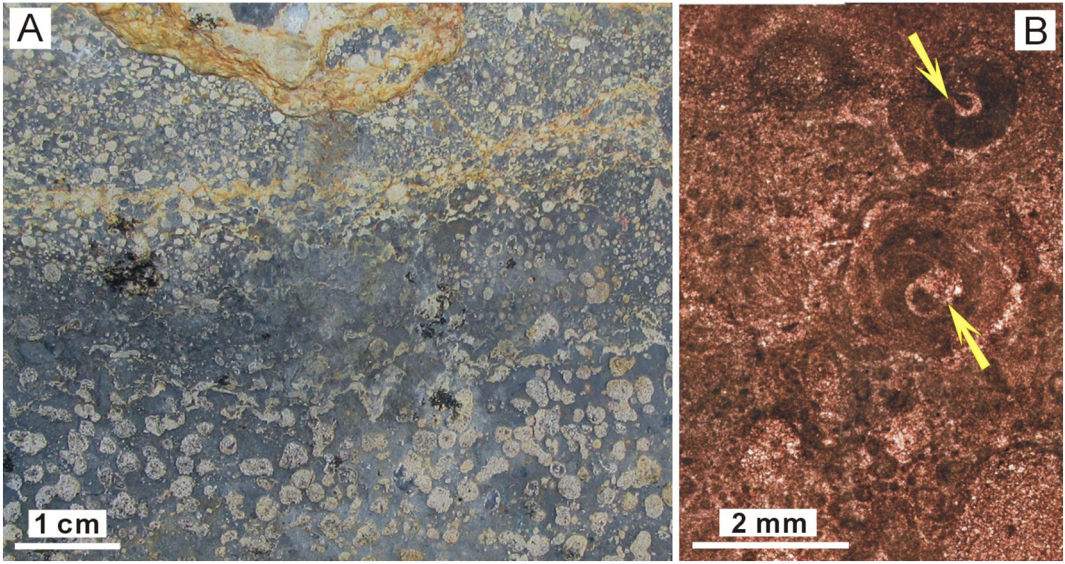

Figure 8

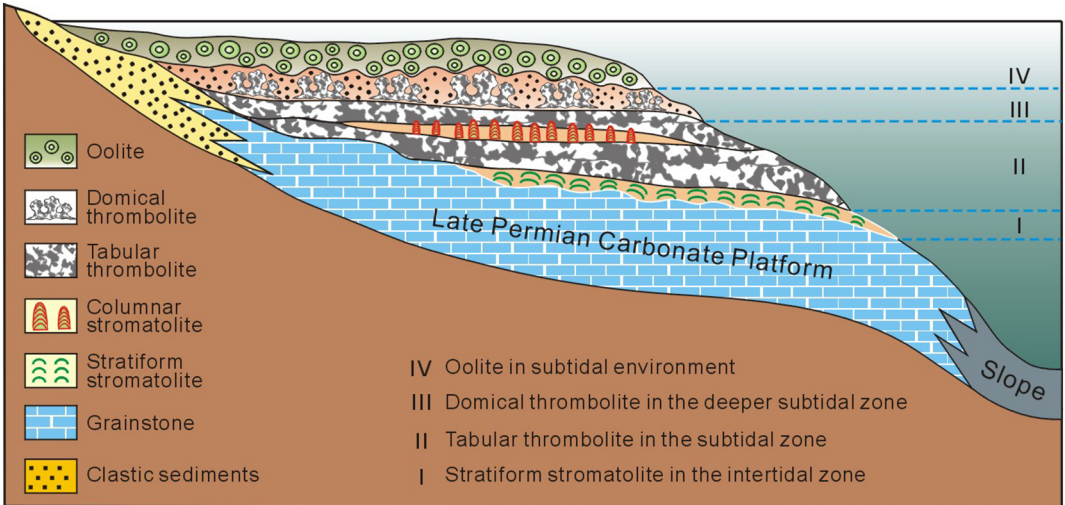
Oolite
Domical thrombolite
Tabular thrombolite
Columnar stromatolite
Stratiform stromatolite
Grainstone
Clastic sediments
Late Permian Carbonate Platform
Slope
IV
III
II
I
IV Oolite in subtidal environment
III Domical thrombolite in the deeper subtidal zone
II Tabular thrombolite in the subtidal zone
I Stratiform stromatolite in the intertidal zone

Figure 9

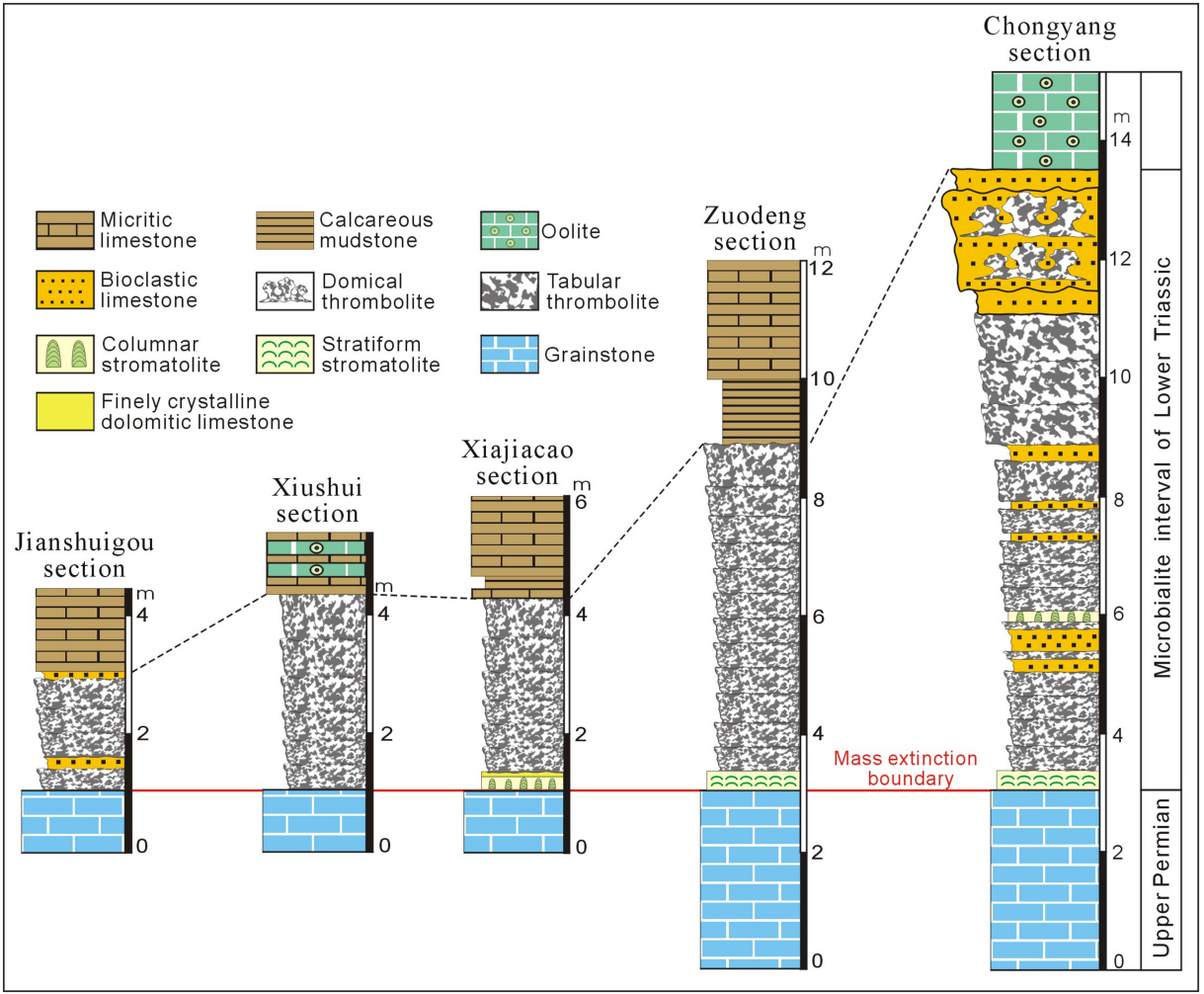
Micritic limestone
Calcareous mudstone
Oolite
Bioclastic limestone
Domical thrombolite
Tabular thrombolite
Columnar stromatolite
Stratiform stromatolite
Grainstone
Finely crystalline dolomitic limestone
Jianshuigou section
Xiushui section
Xiajiacao section
Zuodeng section
Chongyang section
m
Mass extinction boundary
Microbialite interval of Lower Triassic
Upper Permian

Figure 10